Cluster-glass behavior in the two-dimensional triangular lattice Ising-spin compound $Li_2Mn_3O_7$

Rahul Kumar, Premakumar Yanda, and A. Sundaresan *

School of Advanced Materials and Chemistry and Physics of Materials Unit, Jawaharlal Nehru Centre for Advanced Scientific Research, Bangalore 560064, India

(Received 15 March 2021; revised 18 May 2021; accepted 2 June 2021; published 16 June 2021)

We present the detailed structural and magnetic properties of $Li_2Mn_3O_7$ from powder x-ray diffraction (XRD), dc susceptibility, heat capacity, ac susceptibility, thermoremanent magnetization, magnetic memory, and exchange bias effect. Rietveld refinement of XRD data reveals that this compound has a rhombhohedral structure composed of a layered triangular lattice. Onset of spin-glass transition was confirmed by dc magnetization and ac susceptibility measurements. Dynamic scaling laws were used to analyze and classify the glassy behavior of the compound. Magnetic field dependence of irreversible temperature follows the Almeida-Thouless line, which is characteristic for an Ising spin-glass system. Fitting of the frequency-dependent freezing temperature with a power law results in $z\nu' = 4.06 \pm 0.06$, which indicates the critical exponent of the sluggish spin dynamics and $\tau_0 = 4.2 \times 10^{-8}$ s is a characteristic time scale for a single spin-flip. Further evidence of cluster-glass behavior comes from the frequency dependence of the freezing temperature fitted with the Vogel-Fulcher law, which considers interaction between bigger magnetic entities. Values of fitting parameters are $E_a/k_B = 27.62$ K and $T_0 = 9.57$ K, which confirm cluster-glass behavior. The presence of magnetic relaxation below freezing temperature and the magnetic memory effect confirms the nonequilibrium dynamics of the system through a number of metastable states. Moreover, observation of the exchange bias effect reflects the presence of intrinsic phase inhomogeneity. These results indicate that the triangular lattice causes a disordered ground state as a result of competing exchange interactions.

DOI: 10.1103/PhysRevB.103.214427

I. INTRODUCTION

In the last few decades, the unusual magnetic properties shown by low-dimensional compounds have received great attention from the scientific community after the discovery of superconductivity in cuprates at relatively high temperatures [1]. The presence of exotic magnetic properties at low temperatures makes the study of a quasi two-dimensional triangular lattice quite interesting. Compounds showing spin-glass behavior are at the center of research to study the sluggish dynamics of spins, exchange bias effect, magnetic memory effect, and relaxation behavior, which reflects the attraction of current research towards new quantum phenomena [2–5]. The spin-glass state can be classified quantum mechanically as a state having a large number of degenerate ground states which has spins frozen in random directions below a critical temperature [6]. This nonequilibrium state arises because of frustration which can originate from the geometry or competing exchange interactions present in the system [7]. In continuation, cluster-glass is a system which shows spin-glass like dynamic behavior but fundamental blocks responsible for such behavior are larger spin entities rather than the atomic spin which is responsible for spin-glass. Perfect examples of these kinds of systems can be expected from random distributions of diluted magnetic impurities in noble metal or nonmagnetic oxides and lattices having geometrical frustration which hinder the derogation of energy. Some systems may have frustration as a result of competition between nearest-neighbor (NN) and next-nearest-neighbor (NNN) interactions [8]. Triangular geometry having antiferromagnetically coupled magnetic atoms is at the forefront to study frustration, as there may be a large number of ground states due to competing near-neighbor interactions. Comprehensive experimental and theoretical research has been done to search for a novel minimum-energy state without any magnetic order. Upon considering interactions beyond next-neighbor exchange, a ground state with spin disorder can be realized in a triangular lattice; as predicted in recent theories [9].

Members of the lithium-based manganese oxide family are rich in magnetic properties, which is evident from the spin-glass behavior in spinel $LiMn_2O_4$ [10] and antiferromagnetic ordering in a honeycomb lattice of Li_2MnO_3 [11]. But extensive study of the magnetic properties of this family has not been reported. The unconventional magnetism shown by the family members motivated us to examine the magnetic properties of $Li_2Mn_3O_7$. In this report, cluster-glass behavior of $Li_2Mn_3O_7$ has been established by means of various equilibrium and nonequilibrium dynamics experiments. The glassy behavior of the system can be attributed to its fascinating triangular lattice geometry in the *ab* plane. The weak interlayer coupling and ABCABC stacking of triangular layers along the *c* axis make it a potential candidate to study low-dimensional magnetism. Coexisting ferromagnetic and antiferromagnetic nanoclusters are suggested from the presence of the exchange bias (EB) effect.

*sundaresan@jncasr.ac.in

TABLE I. Crystallographic spatial parameters obtained from the Rietveld refinement of $Li_2Mn_3O_7$. Space group = $R-3m$, V = 102.469(2) Å^3, χ^2 = 1.6 %, Bragg R factor = 3.47 %, R_f = 3.06 %.

Atom	Wyckoff symbol	x	y	z
Li	3b	0	0	0.5
Mn	3a	0	0	0
O	6c	0	0	0.2654(5)

II. EXPERIMENTAL PROCEDURE

The chemical sol-gel method was adapted to prepare polycrystalline samples of $Li_2Mn_3O_7$. In the first step, Li_2CO_3 and Mn_2O_3 were dissolved in diluted nitric acid kept at 100°C. After getting a transparent solution, the temperature of the solution was reduced to 80°C and citric acid was added to the solution with constant stirring. The resulting solution was kept at 80°C for 6 h so that a gel was formed, which was further heated at 200°C in air for 12 h. As-prepared powder was ground and heated at 600°C for 12 h in an oxygen atmosphere to remove extra carbon, nitrogen, etc. Then the powder was pressed into pellets and sintered at 700°C for 24 h in air. Room-temperature x-ray diffraction (XRD) data were collected from a PANalytical Empyrean alpha-1 diffractometer using monochromatic Cu Kα_1 radiation of wavelength λ = 1.5406 Å. dc magnetization, magnetic memory, magnetic relaxation, and EB experiments were performed using a Magnetic Property Measurement System (MPMS-SQUID; Quantum Design, USA), while ac susceptibility and heat capacity measurements were carried out using a Physical Property Measurement System (PPMS; Quantum Design). Heat capacity measurement was carried out using thermal relaxation calorimetry on a small pellet of $Li_2Mn_3O_7$ at constant pressure, which was mounted on a sample platform of a heat capacity puck (PPMS) with Apiezon N-grease for better thermal contact. First, we measured the heat capacity of the grease without the sample, which was subtracted from the former to obtain the heat capacity of the sample [12].

III. RESULTS AND DISCUSSION

A. X-ray diffraction and crystal structure

Phase purity of the prepared sample was confirmed by structural analysis of the XRD pattern using the Rietveld refinement method in the FULLPROF package [14]. Initial structural parameters for the refinement were taken from Ref. [13]. From a literature review, we were aware that two different space groups are reported for $Li_2Mn_3O_7$: $R-3m$ [15] and $Fd-3m$ [13]. Upon performing structural fitting with both space groups, $R-3m$ was shown to have a relatively lower goodness of fit (χ^2 = 1.6 %), which is evident in Fig. 1 and, hence, was adapted as a possible crystal structure solution. The obtained lattice parameters from Rietveld refinement, $a = b$ = 2.8902(2) Å and c = 14.1645(2) Å, are in good agreement with the previous report [13]. Arrangements of all atoms in the unit cell are shown in Fig. 2(a) and their coordinates in the unit cell are listed in Table I. The structure of $Li_2Mn_3O_7$ consists of edge-sharing regular octahedra of MnO_6 [edge length = 3.8362(3) Å] and LiO_6 [edge length = 4.3360(8) Å]. The basal and top planes of the unit cell are composed of MnO_6 octahedra only. The Mn ions form equilateral triangle layers in the *ab* plane which are stacked in an ABCABC manner along the *c* axis as shown in Fig. 2(b). Along the *c* axis the interlayer distance between adjacent magnetic layers is more than 5 Å, which rules out any magnetic coupling between interlayer ions through direct exchange interactions. So, magnetic properties of the system will be controlled by intralayer interactions. Figure 2(c) shows the arrangement of Mn-ions in the triangular lattice. The intralayer distance between Mn-Mn atoms is 2.8922(7) Å and the bond angle Mn-O-Mn is 95.41°. According to the Goodenough-Kanamori rules, if the angle between next-to-nearest positive ions is 90°, mediated by nonmagnetic ions, then ferromagnetic interaction will be favored. Any deviation from right angle towards 180° will result in antiferromagnetic interactions. The presence of weakly coupled layers separated by nonmagnetic Li octahedra makes $Li_2Mn_3O_7$ an ideal platform to study quasi-two-dimensional systems, and frustration

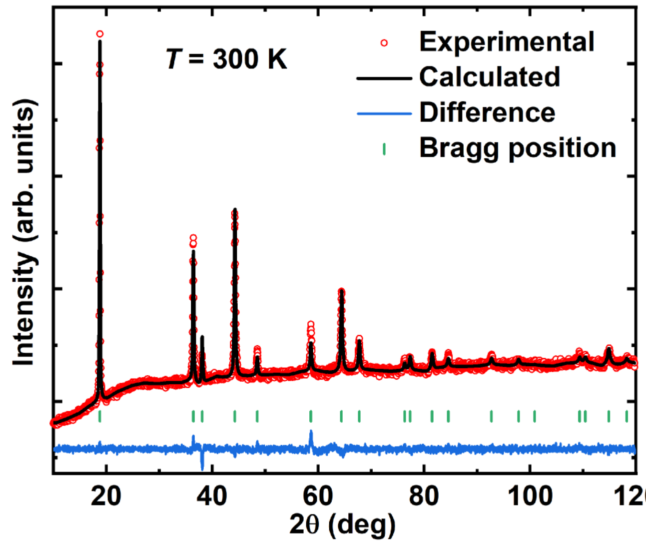

FIG. 1. Rietveld refined room-temperature x-ray diffraction data for $Li_2Mn_3O_7$.

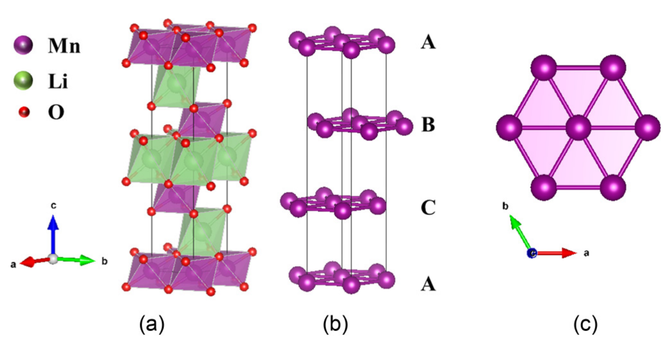

FIG. 2. (a) Crystal structure of $Li_2Mn_3O_7$. Lithium and manganese octahedra are represented in green and purple, respectively. (b) Stacking of a triangular lattice composed of Mn-ions along the *c* axis in the ABCABC manner (c) Projection of the triangular lattice in the *ab* plane.

between various exchange interactions can lead to degenerate ground states.

B. dc magnetization

Temperature-dependent dc magnetic susceptibility was measured under zero field-cooled (ZFC) and field-cooled (FC) protocols with different magnetic fields. For $H = 100$ Oe, both ZFC and FC measurements have a broad peak near $T \sim 12$ K and bifurcation starts well above the peak temperature and continues up to the lowest temperature of measurement, which is shown in Fig. 3(a). The temperature at which bifurcation occurs is known as the irreversible temperature, denoted as T_{irr}, which is the beginning of thermomagnetic irrreversibility. In line with previous published reports [16], bifurcation of ZFC and FC curves at lower temperatures can be a sign of spin-glass or superparamagnetic states. To unfold the behavior of susceptibility with respect to an applied magnetic field, ZFC-FC measurements were done for various magnetic fields ranging from 50 to 1000 Oe. As an outcome, we found that the broad peak temperature as well as the bifurcation temperature decreases with an increase in magnetic field, indicating the presence of a spin-disorder state. As the field increases, the absolute value of the moment also increases and the broad peak in ZFC curve starts to become comparatively narrower. Also, the difference between ZFC and FC curves at low temperatures increases with an increase in magnetic field, which is a direct consequence of the fact that ferromagnetic interactions become more favorable with an increase in magnetic field. The shifting of T_{irr} towards lower temperatures suggests the presence of a frozen spin-glass state below the bifurcation temperature [2]. Although ZFC curves show anomaly near 12 K, the Curie-Weiss law is valid only after 200 K, which is evident in Fig. 3(b). Deviation of ZFC curve from the Curie-Weiss law below 200 K may be due to short-range magnetic fluctuations or low-dimensional ordering [1]. In the high-temperature region, inverse susceptibility (for $H = 100$ Oe) is fitted by the Curie-Weiss law,

$$\chi = \frac{C}{T - \theta_{\mathrm{CW}}},$$

where C is the Curie constant while θ_{CW} is the Curie-Weiss temperature. As a result of the Curie-Weiss law fitting, the effective paramagnetic moment (μ_{eff}) per formula unit turns out to be 6.74 μ_B, which is very close to the theoretical value of 6.72 μ_B. The value of the Curie-Weiss temperature (θ_{CW}) obtained from fitting is $-18.716(5)$ K and the value of the peak temperature (T^*) is 11.59 K. In the case of a glassy compound, θ_{CW} stands for the sum of all kinds of magnetic interactions, so its small magnitude represents competition between ferromagnetic and antiferromagnetic interactions. The frustration parameter ($f = |\theta_{\mathrm{CW}}|/T^*$) is found to be 1.61, which reveals that the sample is moderately frustrated [17].

A change in T_{irr} versus the magnetic field can be fitted with the Almeida-Thouless (AT) line, which is characteristic of strong irreversibility in the H-T phase diagram [18]. The AT line represents the paramagnetic to spin-glass transition which is usual for the Ising spin system. According to mean-field scaling theory, the AT line can be represented by a general

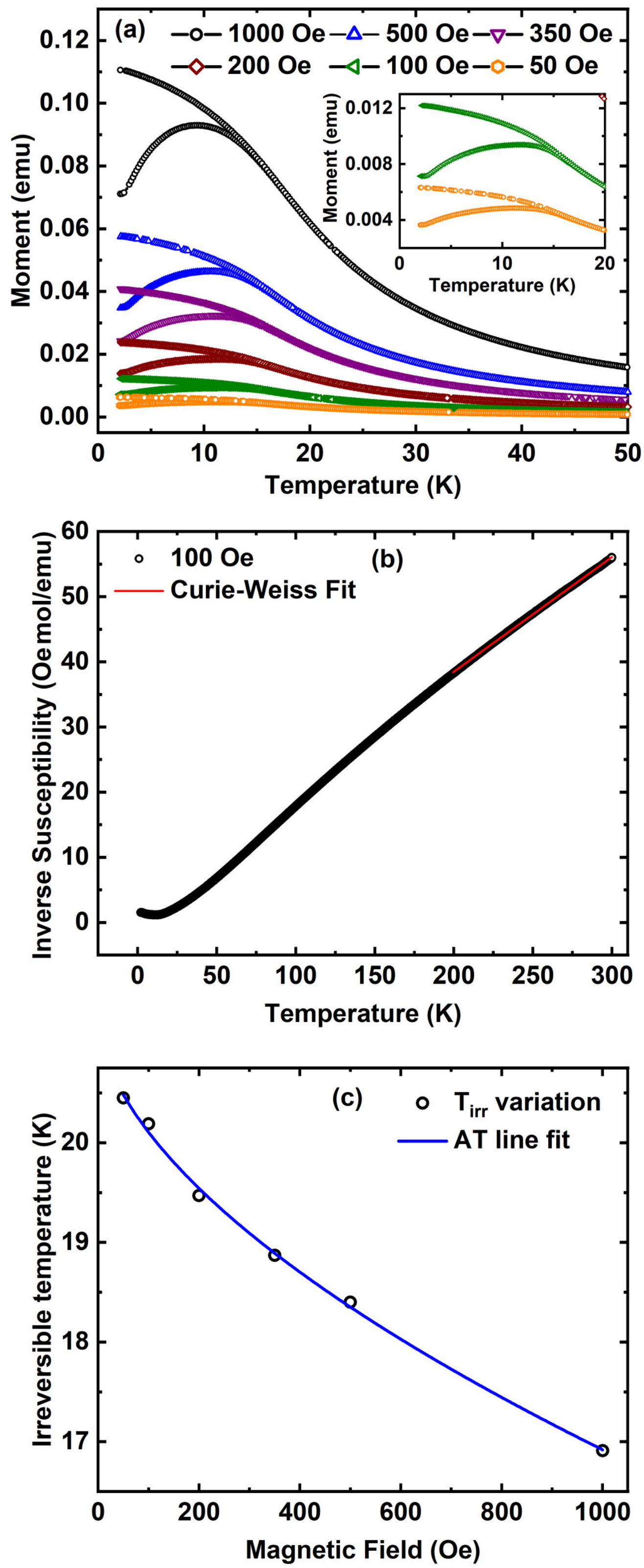

FIG. 3. (a) Temperature-dependent zero field-cooled (ZFC) and field-cooled (FC) dc magnetism under an applied magnetic field ranging from 50 to 1000 Oe. The lower curve for every field represents ZFC, while the upper branch represents FC. Inset: Enlarged view of ZFC and FC curves measured at 50 and 100 Oe. (b) Inverse susceptibility versus temperature. (c) Irreversible temperature at different magnetic fields fitted with the AT line equation.

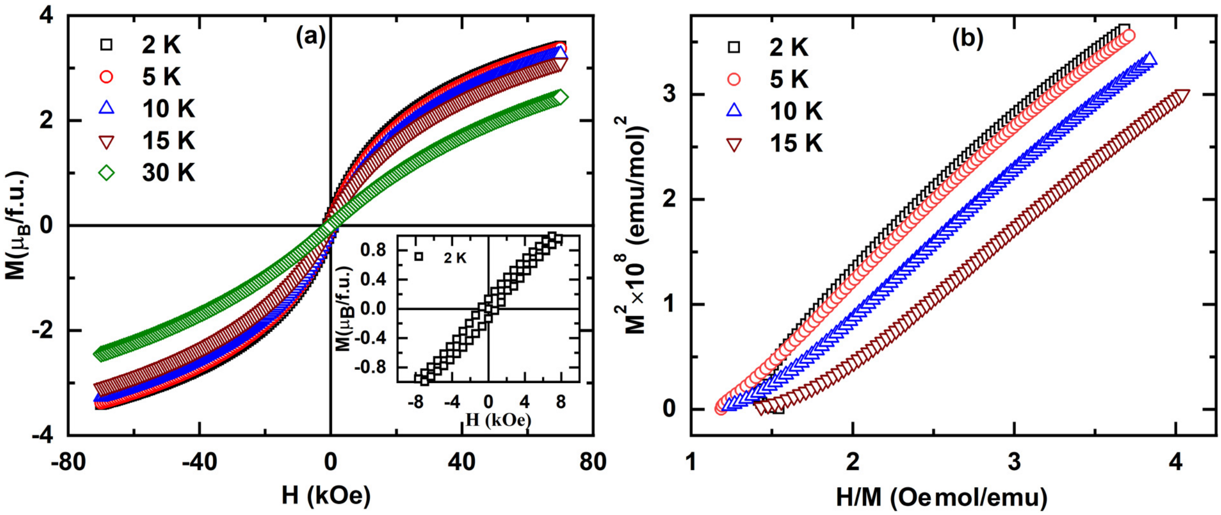

FIG. 4. (a) Isothermal magnetization at 2, 5, 10, 15, and 20 K. Inset: Hysteresis at 2 K. (b) Arrott plots at different temperatures.

equation [18],

$$T_{\mathrm{irr}}(H) = T_{\mathrm{irr}}(0)(1 - CH^n),$$

where $T_{\mathrm{irr}}(0)$ is the bifurcation temperature for zero magnetic field, C is a constant, and n has a theoretical value of $2/3$ for a spin-glass system. Experimental data fitted with the AT line are shown in Fig. 3(c). The obtained value of $T_{\mathrm{irr}}(0)$ is 21.23(8) K and the value of n is 0.58 ± 0.06, which is near to its theoretical value [18].

C. Isothermal magnetization

Figure 4(a) shows isothermal magnetization experiments carried out at different temperatures. In the high-temperature region, the curve is linear (not shown), which illustrates that it is paramagnetic. Upon decreasing the temperature, the curve evolves into an S-type curvature which is more pronounced at low temperatures. At the lowest temperature of measurement ($T = 2$ K), it shows a hysteresis loop with a coercive field of value $\sim$−850 Oe. Also, it is evident from the isothermal magnetization curves that the value of magnetization even at 70 kOe is lower than the saturation magnetization. The lesser value of magnetization at 70 kOe, weak hysteresis of the compound at $T = 2$ K, and S shape of the magnetization suggest low-temperature spin-glass behavior [19]. Also, according to the Ginzburg-Landau mean-field theory, the internal field H depends on the third power of magnetization. Near the magnetic phase transition, the dependence of magnetization can be written as [20]

$$M^2 = \frac{1}{4b}\frac{H}{M} - \frac{a}{2b}\epsilon,$$

where a and b are material-dependent constants, $\epsilon = \frac{T - T_C}{T_C}$ is a dimensionless measure of the transition temperature, while T_C represents the transition temperature of long-range ordering. The parameter $\epsilon > 0$ corresponds to $T > T_C$, while $\epsilon < 0$ corresponds to $T < T_C$. So, a positive intercept on the M^2 axis will be a confirmation of long-range ordering. Figure 4(b) depicts Arrott plots for the magnetic field $H \leqslant 70$ kOe and temperature range $2\ \mathrm{K} \leqslant T \leqslant 15$ K. It is evident from the figure that there is strong curvature towards H/M axis and there is no intercept on the positive M^2 axis. This again confirms the absence of spontaneous magnetization in the compound [21].

D. Heat capacity

Figure 5 represents the temperature-dependent heat capacity divided by the temperature data for the temperature range 3–50 K in the absence of a magnetic field. No sharp anomaly is observed in the heat capacity down to 3 K, which shows that there is no long-range ordering in the compound. The sharp decrease in C_P/T versus T below 10 K is representative of the Schottky anomaly. According to the Schottky postulate [22], the electronic system of some atoms can split in the presence of a crystal field. In the case of a free-ion, the electronic charge distribution should be spherically symmetrical in space. However, when an atom is present in a crystal, a

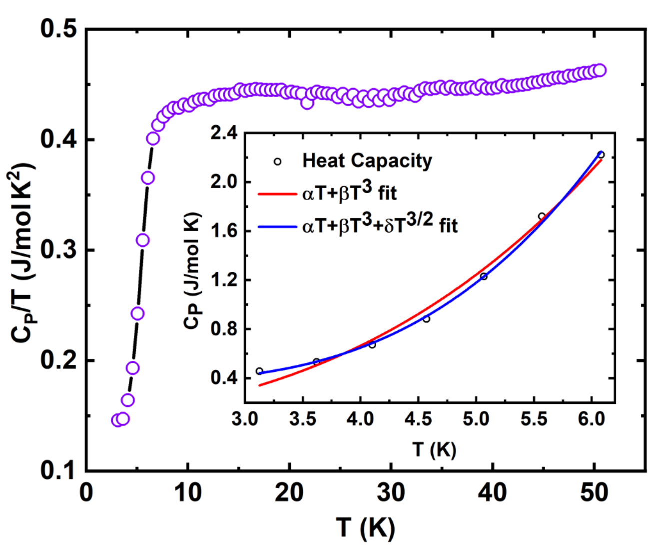

FIG. 5. C_P/T versus T in the absence of a magnetic field between 3 and 50 K. Inset: Fitting of the low-temperature heat capacity with the equations described in the text.

symmetrical distribution of charge on the ion is altered by the charge distribution on neighboring atoms. Lobes or any other shapes representing the charge distribution directed towards other atoms will be elevated higher in energy compared to other shapes which are directed in between the atoms. Typically, the Schottky anomaly is a bell-shaped peak skewed towards high temperatures. The temperature of the peak is related to the separation between electronic levels of the atom while the peak amplitude represents the ratio of degeneracy of the levels. In the present case, Mn^{4+} ions have valance electrons in $3d$ orbitals which are directional in nature and their degeneracy can be lifted by the crystal field energy.

In the low-temperature region, we tried to fit the data by $C_P(T) = \gamma T + \beta T^3$, where γ is a Sommerfield coefficient representing the electronic contribution and β represents the phononic or lattice contribution. The data could not be fitted well with this expression. But after adding a magnetic term $\delta T^{3/2}$ in the specific heat expression, the data could be fitted very well, which is shown in the inset of Fig. 5. In the specific heat capacity expression, the $T^{3/2}$ term characterizes a ferromagnetic or spin-glass system [23,24]. Since in Sec. III B we have ruled out the presence of long-range magnetic ordering, this term supports our claim of glassy behavior of the compound. Using the value of β obtained from the heat capacity fit, the Debye temperature (θ_D) can be calculated as $\theta_D = (12\pi^4 RN/5\beta)^{1/3}$, where R is the universal gas constant and N is the number of atoms per formula unit. From fitting, we get $\beta \simeq 19.4$ mJ/mol K^4 and hence $\theta_D \sim 152$ K.

E. AC susceptibility

To understand the spin dynamics of the compound, a frequency (51 to 9997 Hz)- and temperature-dependent (2 to 20 K) ac magnetic susceptibility experiment was performed to probe the response of the sample against perturbation caused by a fixed ac magnetic field of 10 Oe. Variation of the real part of the magnetic moment with the temperature is shown in Fig. 6. There is an anomaly at $T_f \sim 12$ K for $\nu = 51$ Hz, which shows a frequency-dependent behavior. It is evident from the figure that there is a shift in the peak position towards higher temperatures due to prolongation of the action time-induced spin relaxation delay and the height of the peak also decreases with an increase in the frequency of the applied excitation wave. This trend establishes the spin-glass behavior of the compound. The Mydosh parameter (S) can be used to analyze the relative peak shift in freezing temperature with respect to frequency and to categorize the compound within different spin-glass systems. The Mydosh parameter is a measure of the sensitivity to the applied frequency, which has a vigorous dependence on the interaction among magnetic entities. In the case of spin-glass systems, the entities have a weak interaction and, as a result, have a stronger sensitivity, while for traditional magnets, magnetic ions have very strong interactions, and to get the detectable shift in the ac susceptibility a very large frequency will be required. The expression for the Mydosh parameter is [7,25]:

$$S = \frac{\Delta T_f}{T_f \Delta \log_{10}(\nu)},$$

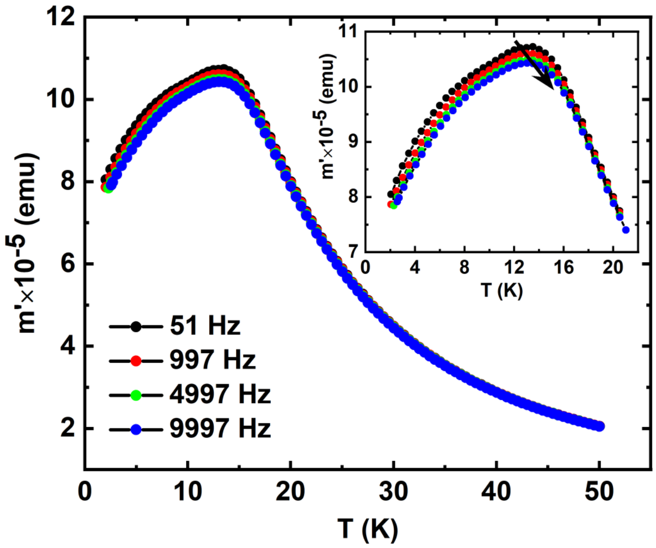

FIG. 6. Variation of the real part of the ac moment measured at different frequencies with the temperature. Inset: Enlarged view of the low-temperature region.

where $\Delta \log_{10}(\nu) = \log_{10}(\nu_2) - \log_{10}(\nu_1)$ and $\Delta T_f = (T_f)_{\nu_2} - (T_f)_{\nu_1}$. For a spin-glass system, the value of S should lie in the range 0.005–0.08 and for a superparamgnetic system it should be greater than 0.2 [6]. To calculate the Mydosh parameter, frequencies ranging from 51 to 9997 Hz were used in our experiment and were taken as ν_1 and ν_2, respectively. The value of the Mydosh parameter turns out to be ∼0.07, which lies in the typical range for a spin-glass system [26–29] and rules out the presence of a superparamagnetic phase.

According to the dynamic scaling theory, the power law is the primary model to analyze the frequency-dependence of the freezing temperature. Critical slowing-down behavior of T_f can be described by the equation [2,6,30]

$$\tau = \tau_0 \left(\frac{T_f - Tg}{T_g} \right)^{-z\nu'},$$

where τ portrays the time-scale of dynamical fluctuation and corresponds to the excitation frequency ν, T_g represents the freezing temperature in the limit $\nu \to 0$, τ_0 corresponds to the single spin-flipping time, z is the dynamical critical constant, and ν' represents the critical exponent of the correlation length as $\zeta = (T_f/T_g - 1)^{-\nu'}$. According to the dynamical scale hypothesis, τ relates to ζ as $\tau \sim \zeta^z$. For smooth fitting of the data, the power law can be readdressed as

$$\log_{10}\nu = \log_{10}\nu_0 + z\nu' \log_{10}\left(\frac{T_f - Tg}{T_g} \right).$$

Here, $\nu = 2\pi/\tau$. The plot of $\log_{10}\nu$ vs $\log_{10}(T_f/Tg - 1)$ shows a typical linear behavior which is evident in Fig. 7(a). The best fitting of the plot with the power law results in $z\nu' = 4.06 \pm 0.06$ and $\tau_0 = 4.2 \times 10^{-8}$ s. These parameters play a decisive role in categorizing spin-glass or cluster spin-glass systems. $z\nu'$ has a value ranging from 4 to 12 for a conventional spin-glass system, while the value of τ_0 typically lies between 10^{-10} and 10^{-13} s [19,31] for a conventional spin-glass system and between 10^{-7} and 10^{-10} s for a

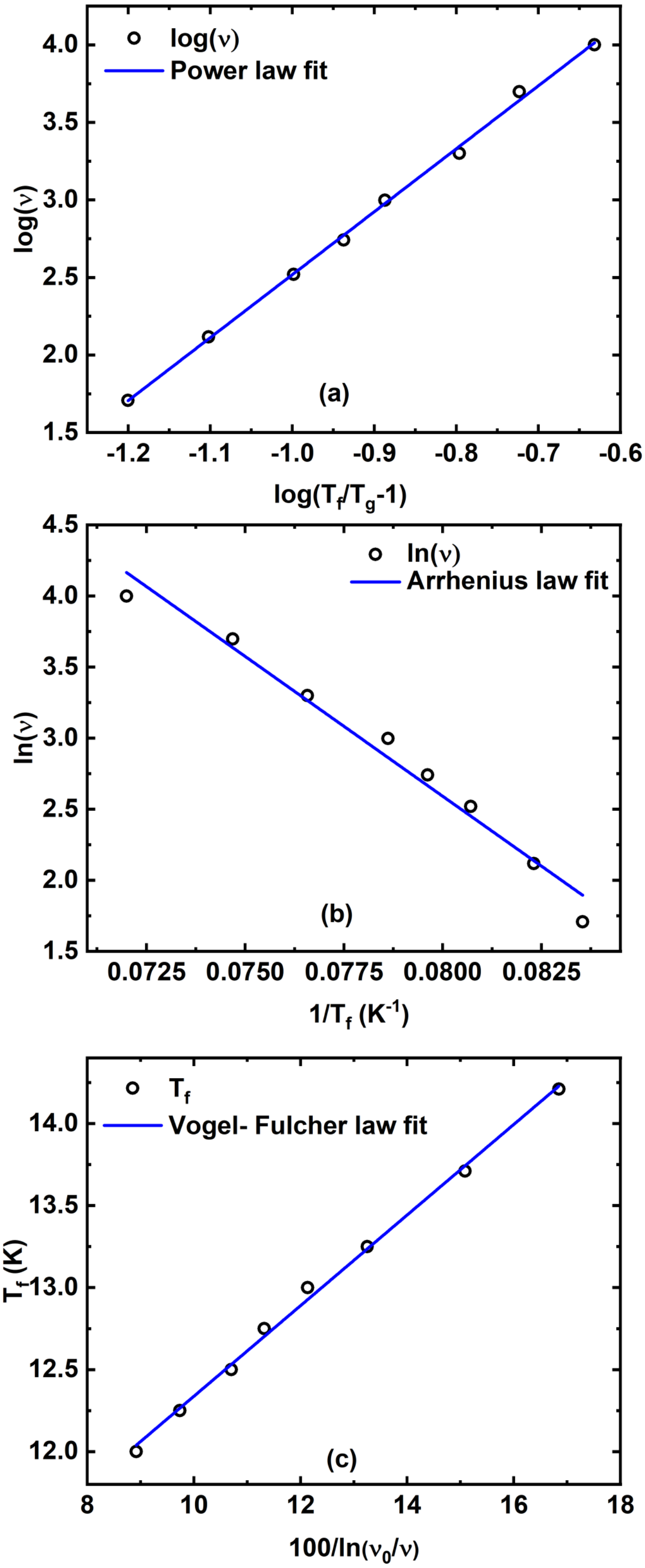

FIG. 7. Fitting of the frequency-dependent freezing temperature with the (a) power law, (b) Arrhenius law, and (c) Vogel-Fulcher law.

cluster-glass system. Parameters obtained from the fitting lie in the range specified for a cluster-glass system. A higher value of τ_0 also supports the presence of interaction between larger magnetic entities rather than small entities.

The existence of interacting clusters can also be confirmed by the Arrhenius law. This law can be fitted only for a system having very weak interactions between the magnetic entities and can be expressed as [2]

$$\tau = \tau^* \exp\left(\frac{E_a}{k_B T_f}\right),$$

where τ^* has the same physical meaning as τ_0, and E_a/k_B represents the mean activation energy of the relaxation barrier. The energy range in which intermediate states become isolated is mapped by the activation energy, while the Arrhenius law, as a whole, measures the time required to conquer the energy barriers with the help of the activation means. The plot of $\ln\nu$ vs $1/T_f$ shows an almost linear behavior [see Fig. 7(b)], which upon fitting with the Arrhenius law results in unphysical values ($\tau^* = 2.2 \times 10^{-20}$ s and $E_a/k_B = 202.36$ K) and backs our claim of a cluster-glass system.

There is one more phenomenological model (Vogel-Fulcher law) which probes the dynamical scaling of the system by taking into account the interaction between relatively larger entities. The Vogel-Fulcher law describes the frequency dependence of the freezing temperature as [6,32]

$$\tau = \tau_0 \exp\left(\frac{E_a}{k_B(T_f - T_0)}\right),$$

where T_0 is a measure of the strength by which magnetic entities in the system interact with each other, known as the empirical Vogel-Fulcher temperature. For convenience of fitting, this law can be rewritten as

$$\ln\left(\frac{\nu_0}{\nu}\right) = \frac{E_a}{k_B(T_f - T_0)},$$

which can further be rearranged as

$$T_F = \frac{E_a/k_B}{\ln(\nu_0/\nu)} + T_0.$$

The plot of T_f versus $100/\ln(\nu_0/\nu)$ (we have used the value of τ_0 from the power-law fitting to calculate ν_0) shown in Fig. 7(c) obeys linear behavior whose slope gives the value of E_a/k_B and whose intercept gives the value of T_0. The values of E_a/k_B and T_0 obtained from the best fit of the plot are 27.62 and 9.57 K, respectively. Along with the nonzero value of T_0, which signifies interaction among clusters, cluster-glass formation is also supported by the close agreement of the Vogel-Fulcher law with our experimental data. Further, we can get insight into the coupling strength of the interaction among magnetic entities of the system by comparing the values of E_a/k_B and T_0. $T_0 \gg E_a/k_B$ indicates strong coupling, while $T_0 \ll E_a/k_B$ stands for a weak coupling strength [33]. In our case, $T_0 \approx 3E_a/k_B$, which lies in the intermediate region, hinting at the presence of finite interaction. Furthermore, the Tholence criterion [34] $\delta T_{Th} = \frac{T_f - T_0}{T_0}$ can also be used to compare different spin-glass systems. For our system, it turns out to be 0.15, which is comparable with other spin-glass systems reported earlier [35]. The agreement of the Tholence criterion acts as a booster to our assertion of a spin-glass system.

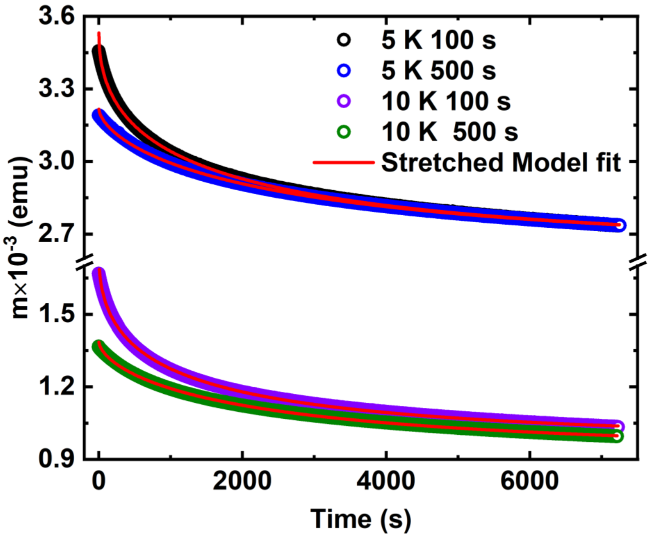

FIG. 8. Relaxation of the magnetic moment at different temperatures, T = 5 and 10 K, for different waiting times, t = 100 and 500 s.

F. Nonequilibrium dynamics

1. Thermoremanent magnetization

Measurement of time-dependent magnetization serves as an additional proof of the glassy behavior of the frustrated system [4,36,37]. In a time frame, the magnetization of the sample can increase or decrease according to the applied magnetic field. To characterize the glassy behavior of the system, a relaxation experiment was carried out at two temperatures, 5 and 10 K, and two waiting times in the FC protocol. The sample was cooled down to the desired temperature below freezing temperature with an applied field of 100 Oe and allowed to wait for 100 and 500 s. Then moment progression was recorded for 7200 s after removing the magnetic field and a well-established stretched exponential model was used to analyze the time-dependent behavior of the moment. The equation describing the stretched exponential model can be written as [29,38,39]

$$m(t) = m_0 - m_g \exp\left[-\left(\frac{t}{\tau}\right)^{\beta}\right],$$

where m_0 represents the intrinsic moment or ferromagnetic component of the compound, m_g stands for the glassy component of the moment, τ is the average relaxation time, and β is the relaxation rate or stretching exponent, whose value lies in the range of 0 to 1 for a spin-glass compound. Fitting of raw relaxation data with the stretched model is shown in Fig. 8. This model does not have any theoretical background, although it has been extensively used to characterize spin-glass systems [40]. For $\beta = 0$, there will be no relaxation in the system and $m(t)$ will have a constant value, while $\beta = 1$ will be an implication of uniform relaxation of the system with a single time constant. The value of β spans the whole range of spin dynamics starting from no relaxation to strong relaxation and it is highly coupled with change in the energy barrier height. For a uniform energy barrier, β attains a value of 1. For all fits, β lies between 0 and 1, which is a clear signature of the presence of intermediate metastable states through which the system is evolving [6,38,41–45]. Values of m_0, m_g, τ, and β obtained from the fitting with the stretched model are summarized in Table II. The presence of coexisting frustrated magnetic and spin-glass phases can also be confirmed by nonzero values of m_0 and m_g. It is evident from the table that τ shows temperature- and time-dependent behavior. The value of τ increases with an increase in the waiting time, while its value decreases with an increase in temperature, which is usual for a glassy system [28,46]. An increase in the value of β with an increase in the waiting time indicates that the heights of all barriers are evolving towards uniformity.

TABLE II. Parameters from the fitting of the relaxation curves at two temperatures for two waiting times.

T (K)	Waiting time	M_0	τ	β
5	100	0.0026(3)	1644(3)	0.49(8)
5	500	0.0026(4)	3044(7)	0.64(6)
10	100	0.0009(7)	1118(2)	0.48(9)
10	500	0.0009(2)	2654(4)	0.61(5)

2. Magnetic memory effect

To explore the low-temperature dynamics behavior of the sample, the magnetic memory effect was also carried out in the ZFC protocol [47,48]. First, the sample was cooled from the paramagnetic region to the desired temperature in the spin-glass region at a constant rate and allowed to dwell at that temperature for 1 h. After dwelling, the sample was cooled to 2 K, and then during warming the magnetization measurement was performed with an applied field of 100 Oe. For reference, the magnetization measurement was carried out without any halt and with a halt at a temperature above the irreversible temperature, i.e., in the paramangnetic region. One can see in the Fig. 9 that there is a dip in the moment at the temperature where cooling was interrupted, which implies

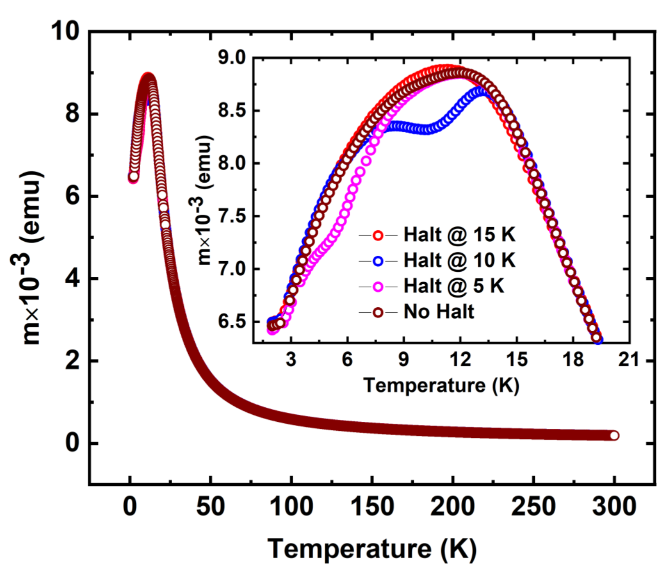

FIG. 9. Memory effect when cooling was halted at T = 5, 10, and 15 K. Inset: Zoomed-in view of the low-temperature data.

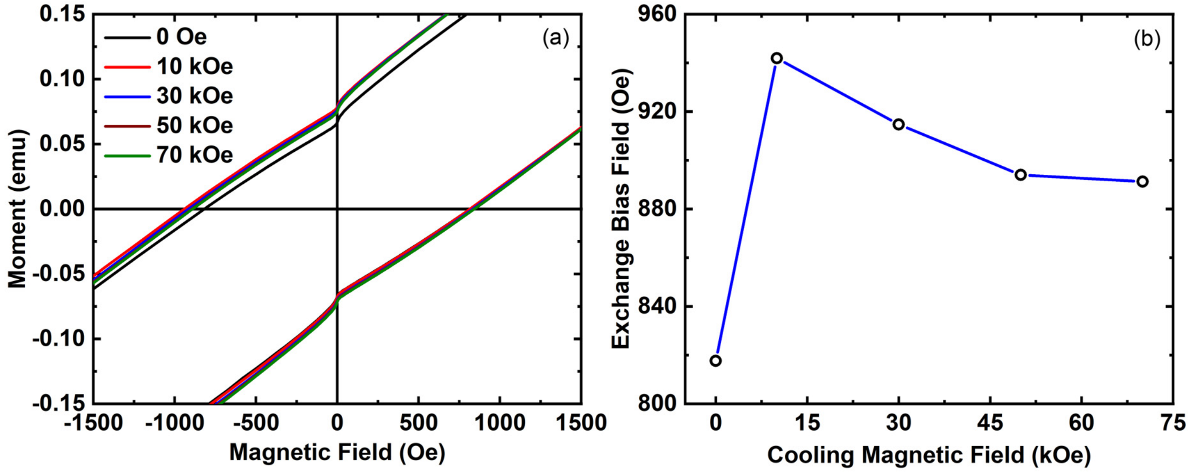

FIG. 10. (a) Isothermal magnetization with different cooling fields at 2 K. (b) Variation of exchange bias field with cooling field.

that the compound retains its memory and suggests that the compound is in a metastable glassy state below the irreversible temperature. The relative magnitude of the dip at 15 K is very low compared to the others as shown in Fig. 9, which implies that frustration is very weak in the region $T_f < T < T_{irr}$ but it dominates below freezing temperature.

G. Exchange bias effect

The EB effect can be seen as a horizontal or vertical shift of the hysteresis loop. It is a replication of the presence of ferromagnetic and antiferromagnetic interfaces. Materials showing the EB effect have found a number of commercial applications which include permanent magnets [49], spin valves [50], and a number of spintronic devices [51]. The presence of the EB effect, besides its cluster-glassy behavior, makes this system of immense fundamental and technological interest to the scientific community. The presence of competition between short-range ferromagnetic interaction and antiferromagnetic interaction can be easily visualized from the increasing behavior of magnetization versus temperature curves shown in Fig. 10.

Generally, the exchange bias effect is observed at the FM/AFM interface, but there are reports of observation of the EB effect at other interfaces like cluster-glass/AFM, FI/FM, and FM/SG, which leads to phase coexistence in the system [52]. The cluster-glass phase has been extensively studied with the help of the EB effect for various systems, with the deduction that cluster-glass has its origin from coexisting ferromagnetic and antiferromagnetic interactions. After confirmation of a cluster-glass system, observation of the exchange bias effect in our system suggests the presence of an additional phase [53]. The small but distinguishable exchange effect shown in Fig. 10(a) in our case can be explained by uniaxial anisotropy along the pinning boundary at the interface [54–56]. The observed variation of the exchange field is also seen for other spin-glass systems [42,53,57], which strengthens our claim of cluster-glass. For the ZFC protocol, the EB effect is not observed, which rules out the presence of finite anisotropy at the interface [58]. The exchange bias effect observed for the FC protocol can be seen as an asymmetrical shift of the coercive field with a change in the cooling magnetic field (H_{CF}) along the direction of the applied field.

In the present system, the hysteresis loop is not getting saturated up to the maximum field of 70 kOe, which may be because of the minor loop effect. But the minor loop is supposed to show significant asymmetry in the vertical direction also. The presence of equal magnetization for the maximum positive and negative fields eliminates the minor loop effect and establishes a conventional EB effect [59,60]. Furthermore, materials showing glassy behavior are not expected to show saturating behavior. Variation of the exchange bias field with respect to the cooling field is shown in Fig. 10(b) and can be explained by considering the local spin arrangement at the interface between the cluster-glass and the AFM states. In the presence of a finite cooling magnetic field, spins will try to align along the direction of the applied field. For $0 \leqslant H_{CF} \leqslant 10$ kOe, ferromagnetic domains have a small size and relatively less magnetization, due to which unidirectional pinning anisotropy has a large magnitude and hence gives rise to an increase in the exchange field magnitude [57]. But with an increase in the magnitude of the cooling field, the magnetic structure of the compound is determined by the increased number of ferromagnetic domains. An increase in the volume of ferromagnetic domains takes place at the expense of unidirectional anisotropy at the FM/SG interface. Hence for $H_{CF} \geqslant 10$ kOe, the exchange field decreases gradually with an increase in the cooling magnetic field. For systems showing glassy behavior, the true nature of the exchange bias effect can be verified by effectively saturated hysteresis loops. So, in accordance with previous reports [42,55], interfacial competitions between FM/SG and AFM/FM interfaces give rise to the EB effect.

IV. CONCLUSION

In conclusion, we have carried out a detailed structural and magnetic study of $Li_2Mn_3O_7$, a quasi two-dimensional system based on a triangular lattice. The temperature-dependent dc susceptibility experiment reveals the onset of a spin-glass transition which is due to competing ferromagnetic and antiferromagnetic interactions. The irreversible temperature is dependent on the magnetic field and follows the AT line. Further justification of the presence of a spin-glass state is given by the ac susceptibility measurements. Various dynamic scaling models are applied to analyze the freezing temperature with the frequency and obtained parameters reveal that the compound attains a cluster-glass state at low temperatures. The relaxation behavior observed in the time-dependent magnetization experiment also confirms the presence of metastable states with nonuniform energy barriers. Glassy behavior is also confirmed by the presence of dips at each dwelling temperature in the magnetic memory experiment. The spin-glass nature of this compound can be attributed to the presence of antiferromagnetically coupled magnetic ions Mn^{4+} at the corners of a triangular lattice, which act as the main driving factor to cause frustration in the system as a result of competition between NN and NNN exchange interactions. Observation of the EB effect suggests the coexistence of FM and AFM nanoclusters in the system. Our experimental results show the formation of cluster-glass behavior at low temperatures but further investigation using neutron diffraction, inelastic neutron scattering, and μSR experiments can improve our understanding of it.

ACKNOWLEDGMENTS

The authors acknowledge the Jawaharlal Nehru Centre for Advanced Scientific Research (JNCASR) for various experimental facilities at Sheikh Saqr Laboratory (SSL) and the International Centre for Materials Science (ICMS). Rahul Kumar is grateful to the Council of Scientific and Industrial Research (CSIR) for Ph.D. fellowship [Grant No. 09/733(0263/2019-EMR-I)].

[1] L. Viciu, Q. Huang, E. Morosan, H. W. Zandbergen, N. I. Greenbaum, T. McQueen, and R. J. Cava, J. Solid State Chem. **180**, 1060 (2007).

[2] K. Binder and A. P. Young, Rev. Mod. Phys. **58**, 801 (1986).

[3] M. C. Cross and P. C. Hohenberg, Rev. Mod. Phys. **65**, 851 (1993).

[4] K. Jonason, E. Vincent, J. Hammann, J. P. Bouchaud, and P. Nordblad, Phys. Rev. Lett. **81**, 3243 (1998).

[5] D. S. Fisher and D. A. Huse, Phys. Rev. B **38**, 373 (1988).

[6] J. A. Mydosh, *Spin Glasses: An Experimental Introduction* (Taylor & Francis, London, 1993).

[7] J. A. Mydosh, J. Magn. Magn. Mater. **157-158**, 606 (1996).

[8] J. S. Gardner, M. J. P. Gingras, and J. E. Greedan, Rev. Mod. Phys. **82**, 53 (2010).

[9] S. Nakatsuji, Y. Nambu, H. Tonomura, O. Sakai, S. Jonas, C. Broholm, H. Tsunetsugu, Y. Qiu, and Y. Maeno, Science **309**, 1697 (2005).

[10] Y.-I. Jang, F. C. Chou, and Y.-M. Chiang, Appl. Phys. Lett. **74**, 2504 (1999).

[11] S. Lee, S. Choi, J. Kim, H. Sim, C. Won, S. Lee, S. A. Kim, N. Hur, and J.-G. Park, J. Phys.: Condens. Matter **24**, 456004 (2012).

[12] J. C. Lashley, M. F. Hundley, A. Migliori, J. L. Sarrao, P. G. Pagliuso, T. W. Darling, M. Jaime, J. C. Cooley, W. L. Hults, L. Morales, D. J. Thoma, J. L. Smith, J. Boerio-Goates, B. F. Woodfield, G. R. Stewart, R. A. Fisher, and N. E. Phillips, Cryogenics **43**, 369 (2003).

[13] E. A. Raekelboom, A. L. Hector, J. Owen, G. Vitins, and M. T. Weller, Chem. Mater. **13**, 4618 (2001).

[14] H. M. Rietveld, J. Appl. Crystallogr. **2**, 65 (1969).

[15] M. M. Thackeray, A. de Kock and W. I. F. David, Mater. Res. Bull. **28**, 1041 (1993).

[16] M. Bandyopadhyay and S. Dattagupta, Phys. Rev. B **74**, 214410 (2006).

[17] A. P. Ramirez, Annu. Rev. Mater. Sci. **24**, 453 (1994).

[18] J. R. L. de Almeida and D. J. Thouless, J. Phys. A: Math. Gen. **11**, 983 (1978).

[19] A. Malinowski, V. L. Bezusyy, R. Minikayev, P. Dziawa, Y. Syryanyy, and M. Sawicki, Phys. Rev. B **84**, 024409 (2011).

[20] A. Arrott, Phys. Rev. **108**, 1394 (1957).

[21] T. K. Nath and A. K. Majumdar, J. Appl. Phys. **70**, 5828 (1991).

[22] B. S. Hemingway and R. A. Robie, Am. Mineral. **69**, 307 (1984).

[23] V. K. Anand, D. T. Adroja, and A. D. Hillier, Phys. Rev. B **85**, 014418 (2012).

[24] E. Gopal, Specific Heats at Low Temperatures (The International Cryogenics Monograph Series) (Springer, Berlin, 1966).

[25] C. A. M. Mulder, A. J. van Duyneveldt, and J. A. Mydosh, Phys. Rev. B **25**, 515 (1982).

[26] D. X. Li, S. Nimori, Y. Shiokawa, A. Tobo, H. Onodera, and Y. Haga, Appl. Phys. Lett. **79**, 4183 (2001).

[27] T. Chakrabarty, A. V. Mahajan, and S. Kundu, J. Phys.: Condens. Matter **26**, 405601 (2014).

[28] B. Maji, K. G. Suresh, and A. K. Nigam, J. Phys.: Condens. Matter **23**, 506002 (2011).

[29] R. S. Freitas, L. Ghivelder, F. Damay, F. Dias, and L. F. Cohen, Phys. Rev. B **64**, 144404 (2001).

[30] P. C. Hohenberg and B. I. Halperin, Rev. Mod. Phys. **49**, 435 (1977).

[31] J. Lago, S. J. Blundell, A. Eguia, M. Jansen, and T. Rojo, Phys. Rev. B **86**, 064412 (2012).

[32] J. Souletie and J. L. Tholence, Phys. Rev. B **32**, 516 (1985).

[33] S. Shtrikman and E. P. Wohlfarth, Phys. Lett. A **85**, 467 (1981).

[34] J.-L. Tholence, Physica B+C **126**, 157 (1984).

[35] P. Beauvillain, C. Chappert, and J. Renard, J. Physique Lett. **45**, 665 (1984).

[36] M. H. R. Mathieu and P. Nordblad, Europhys. Lett. **90**, 67003 (2010).

[37] P. Koželj, S. Jazbec, S. Vrtnik, A. Jelen, J. Dolinšek, M. Jagodič, Z. Jagličić, P. Boulet, M. C. de Weerd, J. Ledieu, J. M. Dubois, and V. Fournée, Phys. Rev. B **88**, 214202 (2013).

[38] A. Bhattacharyya, S. Giri, and S. Majumdar, Phys. Rev. B **83**, 134427 (2011).

[39] S. Chattopadhyay, S. Giri, and S. Majumdar, Europhys. Lett. **98**, 27004 (2012).

[40] R. V. Chamberlin, G. Mozurkewich, and R. Orbach, Phys. Rev. Lett. **52**, 867 (1984).

[41] S. Pakhira, C. Mazumdar, R. Ranganathan, S. Giri, and M. Avdeev, Phys. Rev. B **94**, 104414 (2016).

[42] S. Ghara, B.-G. Jeon, K. Yoo, K. H. Kim, and A. Sundaresan, Phys. Rev. B **90**, 024413 (2014).
[43] C. A. Cardoso, F. M. Araujo-Moreira, V. P. S. Awana, E. Takayama-Muromachi, O. F. de Lima, H. Yamauchi, and M. Karppinen, Phys. Rev. B **67**, 020407(R) (2003).
[44] N. Khan, P. Mandal, and D. Prabhakaran, Phys. Rev. B **90**, 024421 (2014).
[45] D. Chu, G. G. Kenning, and R. Orbach, Phys. Rev. Lett. **72**, 3270 (1994).
[46] D. X. Li, Y. Shiokawa, Y. Homma, A. Uesawa, A. Donni, T. Suzuki, Y. Haga, E. Yamamoto, T. Honma, and Y. Onuki, Phys. Rev. B **57**, 7434 (1998).
[47] P. Bag, P. R. Baral, and R. Nath, Phys. Rev. B **98**, 144436 (2018).
[48] D. Choudhury, P. Mandal, R. Mathieu, A. Hazarika, S. Rajan, A. Sundaresan, U. V. Waghmare, R. Knut, O. Karis, P. Nordblad, and D. D. Sarma, Phys. Rev. Lett. **108**, 127201 (2012).
[49] J. Sort, J. Nogues, S. Surinach, J. S. Munoz, M. D. Baro, E. Chappel, F. Dupont, and G. Chouteau, Appl. Phys. Lett. **79**, 1142 (2001).
[50] V. Kuncser, M. Valeanu, G. Schinteie, G. Filoti, I. Mustata, C. P. Lungu, A. Anghel, H. Chiriac, R. Vladoiu, and J. Bartolome, J. Magnet. Magnet. Mater. **320**, e226 (2008).
[51] J. Sort, S. Suriñach, J. S. Muñoz, M. D. Baró, J. Nogués, G. Chouteau, V. Skumryev, and G. C. Hadjipanayis, Phys. Rev. B **65**, 174420 (2002).
[52] J. Nogués, J. Sort, V. Langlais, V. Skumryev, S. Suriñach, J. S. Muñoz, and M. D. Baró, Phys. Rep. **422**, 65 (2005).
[53] X. K. Zhang, J. J. Yuan, Y. M. Xie, Y. Yu, F. G. Kuang, H. J. Yu, X. R. Zhu, and H. Shen, Phys. Rev. B **97**, 104405 (2018).
[54] S. Karmakar, S. Taran, E. Bose, B. K. Chaudhuri, C. P. Sun, C. L. Huang, and H. D. Yang, Phys. Rev. B **77**, 144409 (2008).
[55] S. K. Giri, A. Poddar, and T. K. Nath, AIP Adv. **1**, 032110 (2011).
[56] M. Ali, P. Adie, C. H. Marrows, D. Greig, B. J. Hickey, and R. L. Stamps, Nat. Mater. **6**, 70 (2007).
[57] R. C. Sahoo, Y. Takeuchi, A. Ohtomo, and Z. Hossain, Phys. Rev. B **100**, 214436 (2019).
[58] C. De, A. K. Nayak, M. Nicklas, and A. Sundaresan, Appl. Phys. Lett. **111**, 182403 (2017).
[59] B. M. Wang, Y. Liu, P. Ren, B. Xia, K. B. Ruan, J. B. Yi, J. Ding, X. G. Li, and L. Wang, Phys. Rev. Lett. **106**, 077203 (2011).
[60] T. Maity, S. Goswami, D. Bhattacharya, and S. Roy, Phys. Rev. Lett. **110**, 107201 (2013).